Anchoring $CoFe_2O_4$ Nanoparticles on N-Doped Carbon Nanofibers for High-Performance Oxygen Evolution Reaction

Tongfei Li, Yinjie Lv, Jiahui Su, Yi Wang, Qian Yang, Yiwei Zhang, Jiancheng Zhou, Lin Xu,* Dongmei Sun, and Yawen Tang*

The exploration of earth-abundant and high-efficiency electrocatalysts for the oxygen evolution reaction (OER) is of great significant for sustainable energy conversion and storage applications. Although spinel-type binary transition metal oxides (AB_2O_4, A, B = metal) represent a class of promising candidates for water oxidation catalysis, their intrinsically inferior electrical conductivity exert remarkably negative impacts on their electrochemical performances. Herein, we demonstrates a feasible electrospinning approach to concurrently synthesize $CoFe_2O_4$ nanoparticles homogeneously embedded in 1D N-doped carbon nanofibers (denoted as $CoFe_2O_4$@N-CNFs). By integrating the catalytically active $CoFe_2O_4$ nanoparticles with the N-doped carbon nanofibers, the as-synthesized $CoFe_2O_4$@N-CNF nanohybrid manifests superior OER performance with a low overpotential, a large current density, a small Tafel slope, and long-term durability in alkaline solution, outperforming the single component counterparts (pure $CoFe_2O_4$ and N-doped carbon nanofibers) and the commercial RuO_2 catalyst. Impressively, the overpotential of $CoFe_2O_4$@N-CNFs at the current density of 30.0 mA cm^{-2} negatively shifts 186 mV as compared with the commercial RuO_2 catalyst and the current density of the $CoFe_2O_4$@N-CNFs at 1.8 V is almost 3.4 times of that on RuO_2 benchmark. The present work would open a new avenue for the exploration of cost-effective and efficient OER electrocatalysts to substitute noble metals for various renewable energy conversion/storage applications.

T. Li, Y. Lv, J. Su, Y. Wang, Q. Yang, Prof. L. Xu, Prof. D. Sun, Prof. Y. Tang
Jiangsu Key Laboratory of New Power Batteries
Jiangsu Collaborative Innovation Centre of Biomedical Functional Materials
School of Chemistry and Materials Science
Nanjing Normal University
Nanjing 210023, China
E-mail: njuxulin@gmail.com; tangyawen@njnu.edu.cn

Prof. Y. Zhang
Jiangsu Optoelectronic Functional Materials and Engineering Laboratory
School of Chemistry and Chemical Engineering
Southeast University
Nanjing 211189, China

Prof. J. Zhou
School of Chemistry and Chemical Engineering
Southeast University
Nanjing 211189, China

Electrocatalytic oxygen evolution reaction (OER, $4OH^- \rightarrow 2H_2O + O_2 + 4e^-$) has stimulated considerable research interests due to its pivotal roles in various sustainable energy conversion and storage devices, such as regenerative fuel cells, solar cells, rechargeable metal–air batteries, and water electrolysis.[1–4] However, the high overpotential and sluggish reaction kinetics of OER dramatically restricts the overall efficiency of energy conversion. Therefore, enormous efforts have been devoted to developing efficient electrocatalysts to reduce the overpotential and expedite the kinetics of the OER.[5–7] To date, commercial electrocatalysts for OER still rely on the precious metal oxides, such as IrO_2 and RuO_2. Unfortunately, their extremely high costs and scarce reserve as well as insufficient long-term stability greatly impede their widespread applications and scalable commercialization in electrochemical energy devices.[8–11] As such, it is extremely important to exploit earth-abundant and low-cost alternative catalysts with high activity and durability comparable or even superior to IrO_2/RuO_2 benchmarks for OER.

It is well-documented that the spinel-type binary transition metal oxides (AB_2O_4, A, B = metal) represent a class of promising candidates for water oxidation catalysis because of their high abundance, low toxicity, rich redox chemistry, and superior stability.[12–17] However, their intrinsically inferior electrical conductivity during electrocatalysis process exerts remarkably negative impacts on their electrochemical performances. To address these issues, one of the effective strategies is to hybridize the AB_2O_4 nanocatalysts with conductive carbon-based substrates (i.e., activated carbon, carbon nanotubes/nanofibers, and graphene) in order to improve their conductivity and electrochemical stability, as well as facilitate charge transfer of the integrated system, thus giving rise to an enhanced OER performance.[18–24] Moreover, heteroatom-doping, such as N-doping, into nanocarbon could effectively improve the electronic conductivity and modulate the electronic structures of the carbon matrix, which is beneficial to boost the OER activity.[25,26] Among various carbon-based supports, 1D carbon nanofibers have been attracting enormous attention in electrochemical energy-related fields due to their large exposed surfaces, shortened distance

for mass diffusion and direct efficient pathway for electron transport.[27–29] Therefore, it is reasonably anticipated that the integration of catalytically active AB_2O_4 nanostructures with highly conductive carbon nanofibers into a nanohybrid could achieve a satisfactory OER performance with high activity and structural robustness. However, for the immobilization of nanocatalysts on carbon supports, previous protocols generally involved multiple complicated synthetic procedures and the nanocatalysts may suffer from aggregation or detachment from the support.[30] To this end, it is highly urgent to explore simple and economical routes to strongly couple AB_2O_4 nanostructures with carbon nanofibers, yet still remains challenging. Fortunately, electrospinning represents a feasible and effective synthetic technique to fabricate metal oxide/carbon-based nanofibers with large surface area, small and uniform grain size, and high morphological uniformity. Moreover, the electrospinning technique is more appealing and promising for practical applications due to its ease of operation, environmentally benign, and large scale production capability.[31–33]
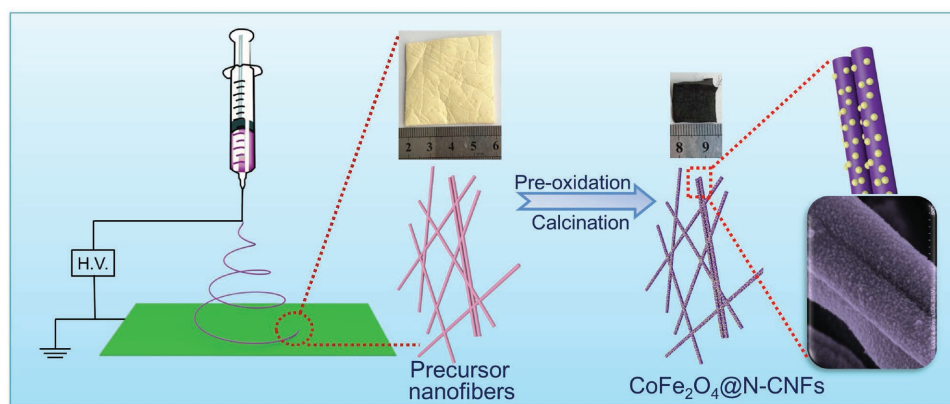
Herein, we demonstrate a facile and reliable electrospinning strategy to synthesize $CoFe_2O_4$ nanoparticle-embedded into N-doped carbon nanofibers (denoted as $CoFe_2O_4$@N-CNFs) with high yield and uniformity, which is schematically illustrated in **Figure 1**. Briefly, the precursor solution containing polyvinylpyrrolidone (PVP), N,N-Dimethylformamide (DMF), $Co(NO_3)_2$, and $Fe(NO_3)_3$ was initially electrospun into a nanofiber membrane. Subsequently, the as-spun uniform polymer nanofibers were stabilized at 250 °C for 3 h in air atmosphere followed by calcination at 600 °C for 3 h in N_2 atmosphere. During the calcination process, the PVP nanofibers would be carbonized into N-doped carbon nanofibers and Co/Fe nitrates would be transformed into spinel-phased $CoFe_2O_4$ nanoparticles. Benefitting from the 1D structural feature and synergy of $CoFe_2O_4$ species of and N-doped carbon nanofibers, the as-synthesized $CoFe_2O_4$@N-CNFs exhibits remarkable OER performance in 0.1 M KOH medium with relatively low overpotential, much improved current density, favorable reaction kinetics, and outstanding long-term stability, as compared with the single-component counterparts (pure $CoFe_2O_4$ and N-CNFs) and the commercial RuO_2 electrocatalyst.

Figure S1 (Supporting Information) presents the typical scanning electron microscopy (SEM) images of the as-prepared polymer nano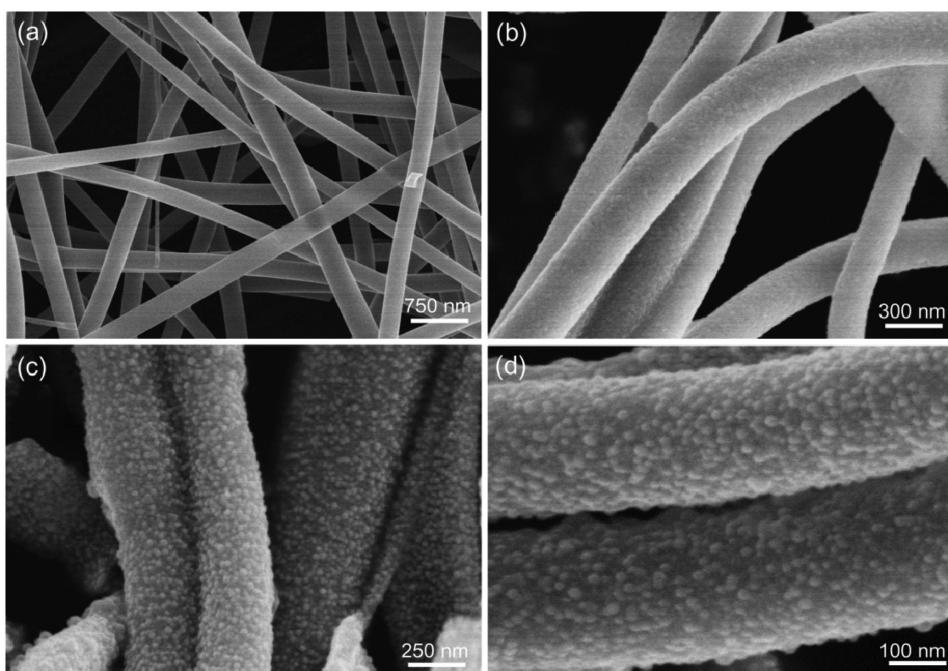fibers. It is clearly observed that the resultant polymer nanofibers with smooth surface and uniform diameters are randomly oriented and highly interconnected, forming 3D continuous networks with mechanical robustness. Such intriguing structural feature is favorable to electron transfer and mass diffusion. Higher magnification SEM images indicate that the average diameter of the polymer nanofibers is around 1.0 µm and the length is up to tens of micrometers. As shown in **Figure 2**a,b the fibers could preserve the original 1D fibrous structure and the interwoven network structure could be still well maintained after the subsequent two-step annealing processes, whereas the average diameter of the obtained $CoFe_2O_4$@N-CNFs is reduced to ≈250 nm, approximately a quarter of that of the parent nanofibers due to the thermal decomposition of PVP matrix and pyrolysis of metal–salt precursors. Closer observations (Figure 2c,d) demonstrate that the surface of the $CoFe_2O_4$@N-CNFs becomes obviously rough and numerous $CoFe_2O_4$ nanoparticles are homogeneously dispersed in the nanofiber supports without any agglomeration.

In consistent with the aforementioned SEM results, representative transmission electron microscopy (TEM) images (**Figure 3**a,b) verify that $CoFe_2O_4$ nanoparticles are uniformly dispersed in the fibrous carbon matrix. Particle size statistics (inset of Figure 3b) of the $CoFe_2O_4$ grains reveals a narrow size distribution and an average size of around 31.4 nm. A high-resolution TEM image (HRTEM) shown in Figure 3c further confirms that $CoFe_2O_4$ nanoparticles are discretely dispersed within the carbon scaffolds, without obvious aggregation. Selected area electron diffraction (SAED) pattern (inset of Figure 3c) of an individual $CoFe_2O_4$ nanoparticle demonstrates the polycrystalline feature of the $CoFe_2O_4$ nanoparticles. The lattice fringe (Figure 3d) recorded from square area marked in Figure 3c is clearly measured to be 0.21 nm, corresponding to interplanar distance of the (400) plane of spinel-phased $CoFe_2O_4$. The high-angle annular dark-field scanning TEM (HAADF-STEM) image and elemental mapping images (Figure 3e) suggest the homogeneous distribution of Co, Fe, O, and C throughout the fibrous nanocomposite.

X-ray diffraction (XRD) pattern of the $CoFe_2O_4$@N-CNFs is presented in **Figure 4**a. All of the diffraction peaks can be attributed to the spinel-type $CoFe_2O_4$, whose unit cell structure is constructed by CoO_4 tetrahedra and FeO_6 octahedra (Figure 4b). The sharp diffraction peaks imply the high crystallinity of the $CoFe_2O_4$. The energy dispersive X-ray spectroscopy (EDS)

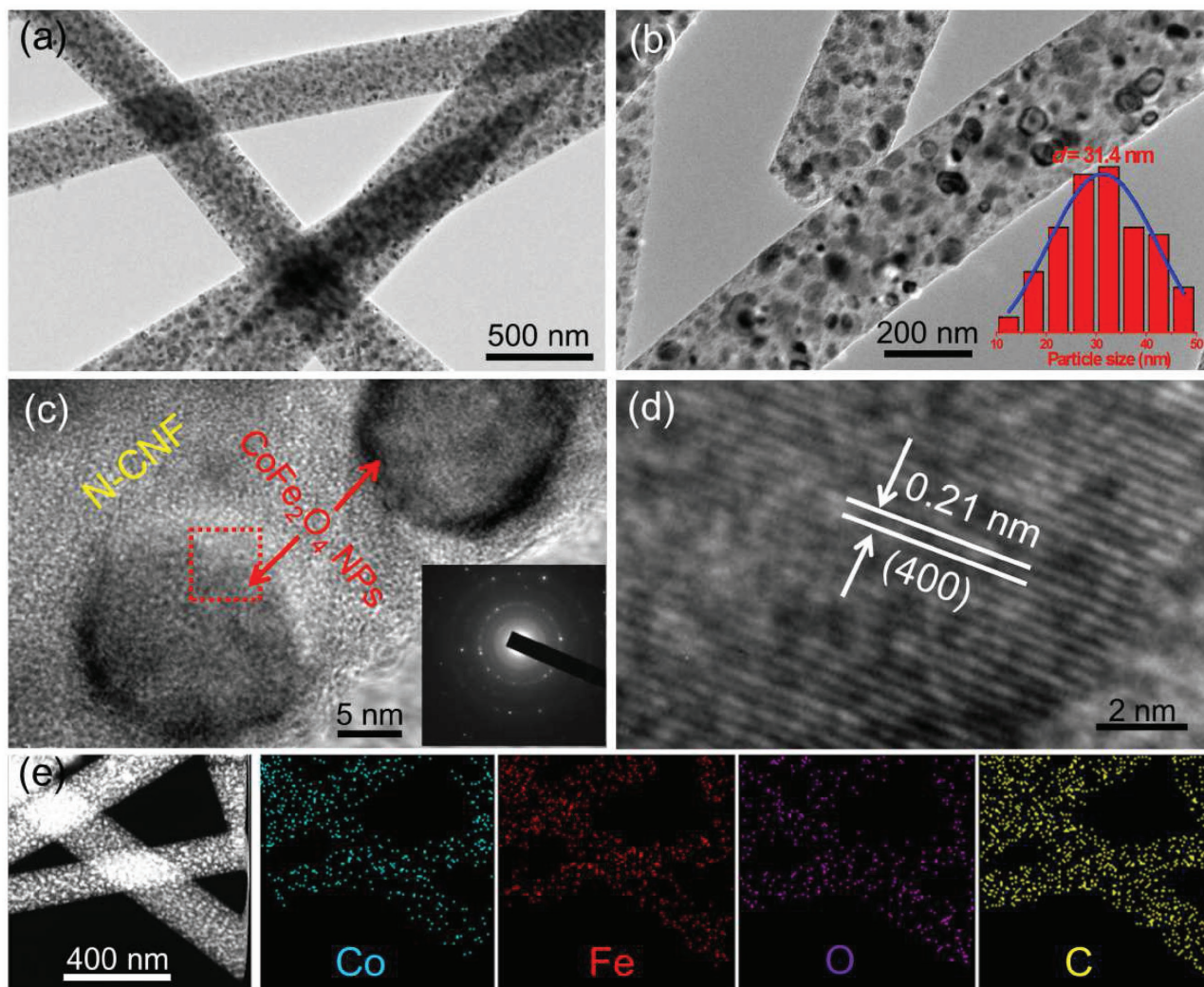**Figure 1.** Schematic illustration of the overall synthesis of the $CoFe_2O_4$@N-CNFs.

**ADVANCED
SCIENCE NEWS**

www.advancedsciencenews.com

**ADVANCED
SCIENCE**
Open Access

www.advancedscience.com

Figure 2. a–d) Representative SEM images of the obtained CoFe$_2$O$_4$@N-CNFs with different magnifications.

shown in Figure 4c suggests the presence of Co, Fe, O, and C in the obtained CoFe$_2$O$_4$@N-CNFs with the Fe/Co molar ratio of ≈2.04, which is in agreement with the stoichiometric ratio of 2. It is noteworthy that the Cu signal comes from the copper grid. The carbon content in the CoFe$_2$O$_4$@N-CNFs acquired from the thermogravimetric analysis (TGA) in Figure 4d is quantitatively to be 4.7 wt%. The degree of graphitization of the carbon nanofibers is investigated by Raman spectrum, as illustrated in Figure 4e. Two well-defined peaks can be observed at 1358 and 1588 cm^{-1}, which are assigned to the D and G bands of carbon materials, respectively. It is well-established that the D band arises from the disordered or defect carbon and the G band originates from the sp^2-hybridized graphitic carbon. The intensity ratio between D band and G band (I_D/I_G) generally reflects the graphitization degree of carbon materials and a lower value to I_D/I_G indicates a higher graphitization degree.[34–38] Here the I_D/I_G ratio of CoFe$_2$O$_4$@N-CNFs is calculated to be 0.83, suggesting a well-crystallized graphitic carbon in the carbon nanofibers. Such a high graphitization degree is beneficial to improve the electronic conductivity of the hybrid nanofibers. The N$_2$ adsorption–desorption isotherms (Figure 4f) of the CoFe$_2$O$_4$@N-CNFs can be categorized as type-IV isotherms with a noticeable hysteresis loop, indicating the presence of mesopores (2–50 nm). The Brunauer–Emmett–Teller (BET) surface area is measured to be 52.9 m^2 g^{-1}.

The chemical compositions and valence states of the constituent elements in the as-fabricated CoFe$_2$O$_4$@N-CNFs are investigated through X-ray photoelectron spectroscopy (XPS) technique. As displayed in **Figure 5**a, the survey-scan spectrum manifests that the sample is composed of Co, Fe, C, N, and O elements. The existence of N can be ascribed to the pyrolysis of PVP during the calcination process.[39,40] The high-resolution Fe 2p spectrum (Figure 5b) exhibits two characteristic

peaks at 711.0 eV (Fe 2p$_{3/2}$) and 724.5 eV (Fe 2p$_{1/2}$) as well as a minor peak at 718.5 eV (shake-up satellite peak of Fe 2p$_{3/2}$), indicating the oxidation state of Fe^{3+}. The high-resolution Co 2p spectrum (Figure 5c) can be deconvoluted into four peaks, which are corresponding to Co 2p$_{3/2}$ (779.6 eV), Co 2p$_{3/2}$ satellite peak (785.8 eV), Co 2p$_{1/2}$ (795.1 eV), and Co 2p$_{1/2}$ satellite peak (801.6 eV), respectively. The presence of Co 2p$_{3/2}$ and Co 2p$_{1/2}$ main peaks and their shake-up satellite peaks suggest the oxidation state of Co^{2+}. The high-resolution C 1s spectrum (Figure 5d) displays a prominent nonoxygenated C−C peak (284.6 eV) and a weak C−O peak (286.2 eV). The C−O peak may be arisen from the covalent coupling between the CoFe$_2$O$_4$ and C support or from some oxygen-containing groups on the surface of the carbon nanofibers. The high-resolution N 1s spectrum (Figure 5e) can be well fitted into four peaks and assigned to the pyridinic N (398.6 eV), pyrrolic N (399.9 eV), graphitic N (400.9 eV), and oxidized N (401.9 eV), respectively. Figure 5f shows the schematic representation of the four types of nitrogen configurations in carbon matrix. The incorporation of N into carbon nanofibers can not only effectively enhance the overall electrical conductivity of carbon nanofibers but also generate some defects or vacancies among carbon nanofibers, therefore, affording numerous active sites for electrocatalysis and thus expediting the reaction kinetics.[41–44]

Inspired by the CoFe$_2$O$_4$ nanoparticles anchored on highly conductive carbon nanofiber networks, the electrocatalytic performance of the as-synthesized CoFe$_2$O$_4$@N-CNF hybrid toward OER was appraised in 0.1 M KOH solution using a standard three-electrode system. For comparison, pure CoFe$_2$O$_4$ (Figure S2, Supporting Information), N-doped carbon nanofibers (N-CNFs, Figure S3, Supporting Information), and commercial RuO$_2$ were also evaluated under the identical measurement conditions. The textural properties of

**ADVANCED
SCIENCE NEWS**

www.advancedsciencenews.com

**ADVANCED
SCIENCE**
Open Access

www.advancedscience.com

Figure 3. a,b) TEM images, c,d) HRTEM images, e) HAADF-STEM image, and elemental mapping images of the $CoFe_2O_4$@N-CNFs. Insets of (b) and (c) show the particle size distribution and SAED pattern of the $CoFe_2O_4$ nanoparticles, respectively.

the $CoFe_2O_4$ and N-doped carbon nanofibers, including N_2 adsorption–desorption isotherms and pore-size distribution curves, are presented in Figure S4 of the Supporting Information. **Figure 6**a shows the typical *IR*-corrected linear sweep voltammetry (LSV) curves of the four catalysts obtained at a scan rate of 5 mV s^{-1} and 1600 rpm rotation rate. It can be clearly seen that the LSV curves of pure $CoFe_2O_4$ and N-CNFs show inconspicuous current densities within the tested potential range, suggesting their negligible activities to OER. In striking contrast, the $CoFe_2O_4$@N-CNF nanohybrid shows a comparable onset potential with the commercial RuO_2 catalyst, highlighting the synergistic effect between $CoFe_2O_4$ and N-CNFs. As we know, the overpotential (η) required to afford a current density of 10.0 mA cm^{-2}, approximately the current density for a 10% efficient solar-to-fuel conversion device, is an important figures-of-merit to evaluate an OER catalyst.[45,46] The η of the $CoFe_2O_4$@N-CNFs to achieve a current density of 10.0 mA cm^{-2} is 349 mV, which is almost identical with that of the commercial RuO_2 catalyst (342 mV). Surprisingly, under the higher current densities, the required overpotentials of the

$CoFe_2O_4$@N-CNFs are significantly lower than those of the commercial RuO_2 catalyst, as shown in Figure 6b. Specifically, the overpotential of $CoFe_2O_4$@N-CNFs at the current density of 30.0 mA cm^{-2} is determined to be 408 mV, which negatively shifts 186 mV as compared with the commercial RuO_2 catalyst. Meanwhile, the $CoFe_2O_4$@N-CNFs can deliver a much higher current density under the same applied potential, as illustrate in Figure 6c. The $CoFe_2O_4$@N-CNFs can attain a current density of 56.68 mA cm^{-2} at 1.7 V, which is 2.6 times higher than that of RuO_2 reference. Similarly, the current density of the $CoFe_2O_4$@N-CNFs reaches a value of 97.50 mA cm^{-2} at 1.8 V, almost 3.4 times of that on RuO_2 benchmark. By using cyclic voltammetry (CV) measurement, the electrochemically active surface areas (ECSAs) of the prepared $CoFe_2O_4$@N-CNFs and commercial RuO_2 catalyst are evaluated by their electrochemical double-layer capacitances (C_{dl}) due to the fact that C_{dl} is proportional to the ECSA. Figure S5a,b (Supporting Information) presents the CV curves of the two catalysts recorded in a non-Faradic potential range under different scan rates. As displayed in Figure S5c (Supporting Information), the C_{dl} value of the
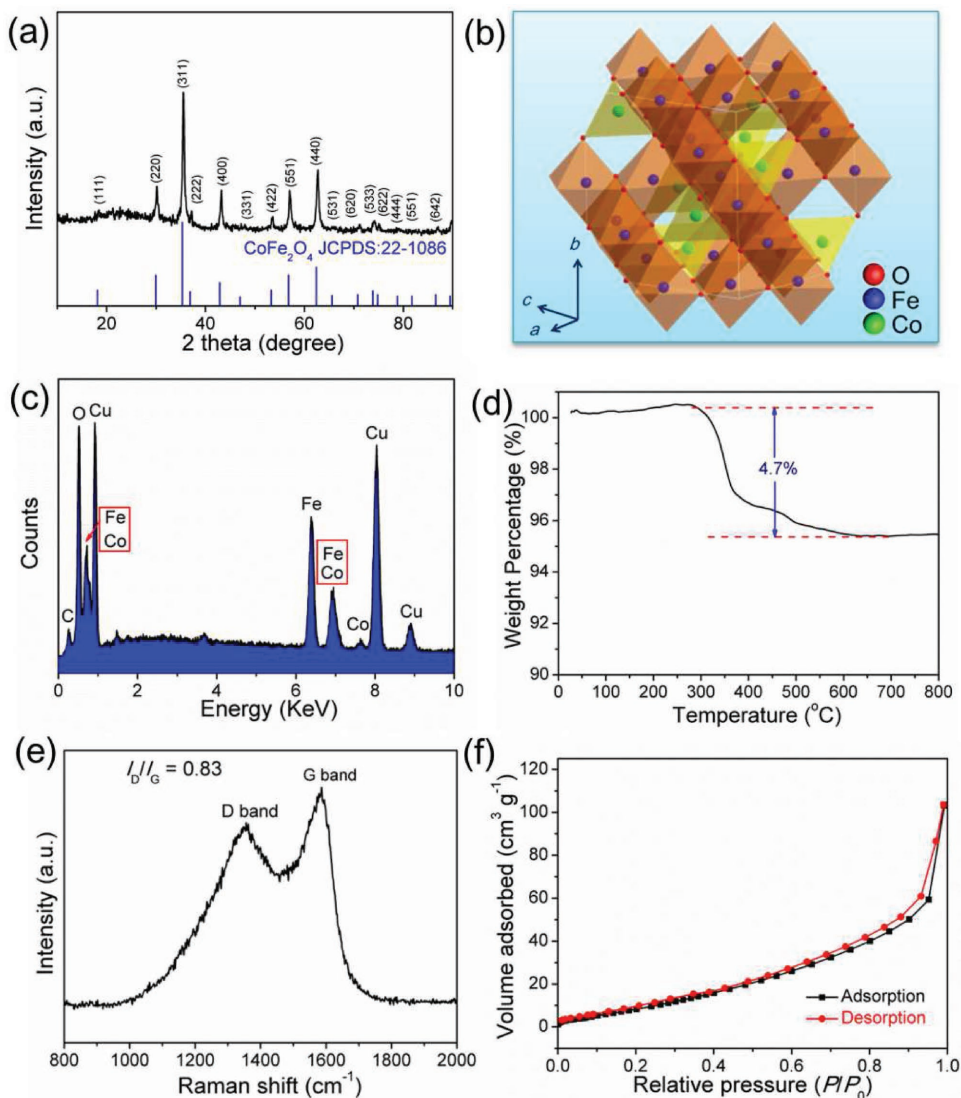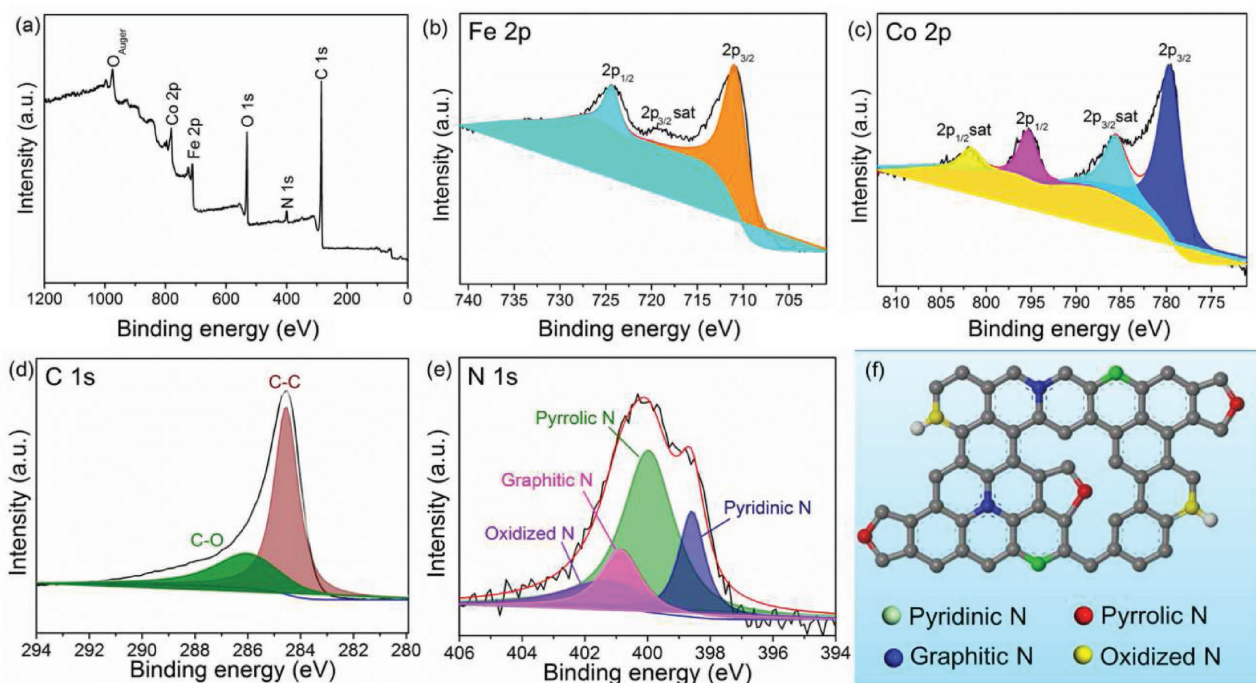
Figure 4. Compositional characterization of the as-prepared $CoFe_2O_4$@N-CNFs. a) XRD pattern, b) crystal structure of spinel-phased $CoFe_2O_4$, c) EDS, d) TGA curve, e) Raman spectrum, and f) N_2 adsorption–desorption isotherms.

$CoFe_2O_4$@N-CNFs is determined to be 20.6 mF cm^{-2}, which is 1.4 times higher than that of the commercial RuO_2 catalyst. This result demonstrates that the synthesized $CoFe_2O_4$@N-CNFs could afford a larger number of catalytically active sites and thus an improved OER activity.

The electrocatalytic kinetics for OER of the $CoFe_2O_4$@N-CNFs and the commercial RuO_2 catalysts are further investigated by Tafel plots, as displayed in Figure 6d. The Tafel slope of the $CoFe_2O_4$@N-CNFs is identified as 80 mV dec^{-1}, which is comparable to that of the RuO_2 catalyst (75 mV dec^{-1}). Moreover, the similar Tafel slope of the two catalysts indicates that both catalysts undergo the same rate-determining step and reaction pathway toward the OER.[47,48] As compared with the previously reported nonprecious metal-based OER electrocatalysts, our $CoFe_2O_4$@N-CNFs show comparable and even better electrocatalytic properties toward OER in basic solution with relatively low onset potential and Tafel slope, as summarized in Table S1 of the Supporting Information.

The long-term stability of an electrocatalyst is also a critical parameter for practical applications. As illustrated in Figure 6e, the LSV curve of the $CoFe_2O_4$@N-CNFs for the OER shows negligible degradation after continuous 1000 CV cycles, indicating its superior operational stability under alkaline test condition. Consistently, the chronopotentiometric curves performed at 1.7 V (Figure 6f) indicate that the current attenuation of the $CoFe_2O_4$@N-CNFs after 40 000 s is merely 7.3%, whereas the RuO_2 suffers great activity deterioration, with a current loss of 39.8% after 40 000 s. Furthermore, as evidenced TEM images shown in Figure S6a,b (Supporting Information), the 1D fiber-like structure of the $CoFe_2O_4$@N-CNFs after the long-term stability test could be well retained and $CoFe_2O_4$ nanoparticles are still well dispersed. Particle size statistics (inset of Figure S6b, Supporting Information) further indicates that the average size of the $CoFe_2O_4$ nanoparticles is still centered at $\approx$32 nm, without obvious aggregation and expansion, thanks to the immobilization effect of carbon nanofiber scaffold.
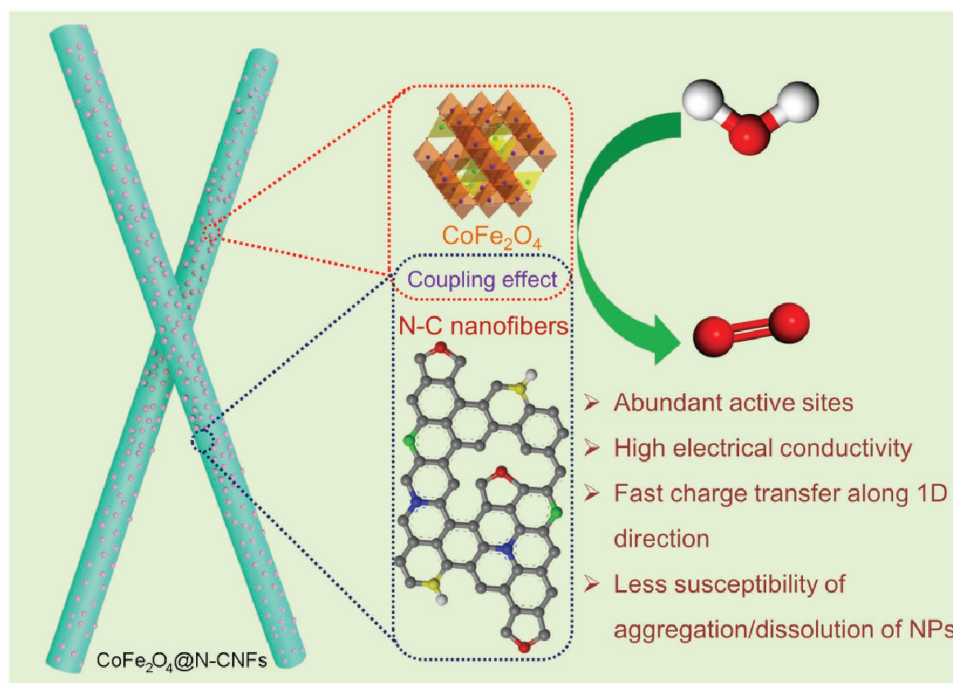
**ADVANCED
SCIENCE NEWS**

www.advancedsciencenews.com

**ADVANCED
SCIENCE**
Open Access

www.advancedscience.com

Figure 5. XPS spectra of the CoFe$_2$O$_4$@N-CNFs. a) Survey scan spectrum, b) Fe 2p region, c) Co 2p region, d) C 1s, e) N 1s, and f) schematic configurations of N with different chemical states in C matrix.

A high-resolution TEM image (Figure S6c, Supporting Information) further confirms that CoFe$_2$O$_4$ nanoparticles are firmly dispersed within the carbon scaffolds. The well-resolved lattice fringe (Figure S6d, Supporting Information) recorded from square area marked in Figure S6c (Supporting Information) is clearly measured to be 0.299 nm, corresponding to interplanar distance of the (220) plane of spinel-phased CoFe$_2$O$_4$. The HAADF-STEM image and elemental mapping images (Figure S6e, Supporting Information) imply the uniform distribution of C, O, Fe, and Co throughout the CoFe$_2$O$_4$@N-CNFs
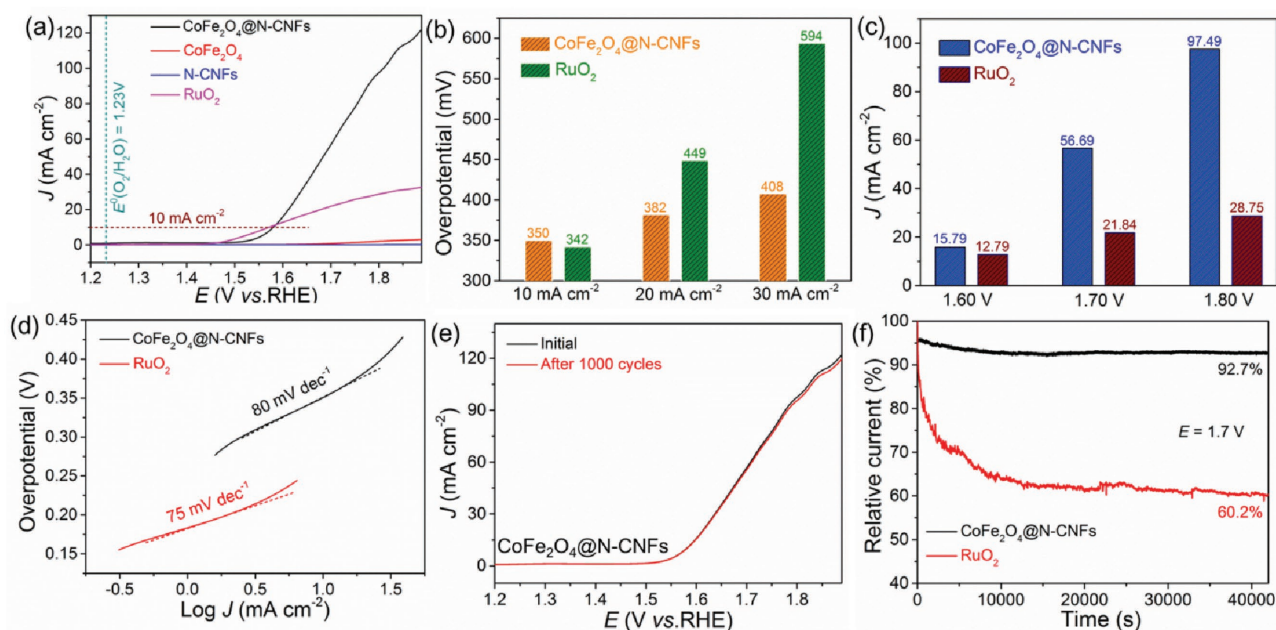
Figure 6. Comparison of OER performances of different catalysts. a) LSV polarization curves, b) required overpotentials derived from OER polarization curves at different current densities, c) current densities achieved at different potentials, d) Tafel plots, e) LSV polarization curves of the CoFe$_2$O$_4$@N-CNFs before and after 1000 cycles, and f) chronopotentiometry curves of the CoFe$_2$O$_4$@N-CNFs and commercial RuO$_2$ catalyst.

ADVANCED
SCIENCE NEWS
www.advancedsciencenews.com

ADVANCED
SCIENCE
Open Access
www.advancedscience.com

Figure 7. A schematic illustration of the structural and compositional advantages of the synthesized $CoFe_2O_4$@N-CNFs as an efficient OER electrocatalyst.

after the long-term stability. All these results unambiguously affirm the structural and chemical stability of the obtained $CoFe_2O_4$@N-CNFs after long-term stability test. Taken together, all above results strongly demonstrate that the synthesized $CoFe_2O_4$@N-CNFs possess superior OER performance with relatively low overpotential, enhanced activity, satisfied kinetics, and better stability, endowing it a promising efficient OER electrocatalyst for future applications.

The outstanding OER performance of the prepared $CoFe_2O_4$@N-CNFs can be mainly attributed to the unique structural feature and the synergistic effect between the well-dispersed tiny $CoFe_2O_4$ nanoparticles and the nitrogen-doped graphitic carbon nanofibers, as illustrated in **Figure 7**. To be specific, (1) the numerous homogeneously distributed $CoFe_2O_4$ nanoparticles could afford a high density of OER active sites on the surface; (2) the hybridization of $CoFe_2O_4$ nanoparticles with nitrogen-doped graphitic carbon could not only remarkably endow the composite with good conductivity for charge transfer during electrochemical process, but also firmly immobilize the $CoFe_2O_4$ nanoparticles, preventing their detachment or aggregation; (3) the nitrogen doping in carbon nanofibers could provide more catalytically active sites for OER; (4) the network constructed by interconnected 1D nanofibers could offer continuous 3D pathways for mass diffusion and electron transport. Furthermore, the strong coupling between $CoFe_2O_4$ nanoparticles and nitrogen-doped carbon nanofibers may give rise to a synergistic effect and thus an improved OER activity. By integrating all above advantages, the as-prepared $CoFe_2O_4$@N-CNFs exhibit impressive OER performance with exceptional activity and excellent stability.

In conclusion, we have presented a simple and scalable electrospinning strategy for the concurrent synthesis of $CoFe_2O_4$ nanoparticles homogeneously embedded in N-doped carbon nanofibers. Compared with the single component counterparts (pure $CoFe_2O_4$ and N-doped carbon nanofibers) and commercial RuO_2 catalyst, the synthesized $CoFe_2O_4$@N-CNFs are demonstrated to be an efficient earth-abundant OER electrocatalyst with a low overpotential, a large current density, a small Tafel slope, and long-term durability in alkaline solution. The improved catalytic performances are believed to originate from the unique 1D structural feature and the synergy between the constituent components. Considering the cost-effectiveness, facile, and reliable fabrication process, and outstanding catalytic performance, the $CoFe_2O_4$@N-CNFs may hold great potential to in future energy conversion and storage devices. More importantly, the present versatile synthetic strategy may stimulate the rational design of other metal oxides/carbon nanofibers through the similar one-step concurrent growth method for diverse applications in the future.

Experimental Section

Synthesis of $CoFe_2O_4$@N-CNFs: For the typical electrospinning synthesis of $CoFe_2O_4$@N-CNFs, 1.0 g PVP (average M_w = 1 300 000, Alfa Aesar) was initially dissolved in 10 mL DMF (Sinpharm Chemical Reagent) with vigorous stirring for 6 h to obtain a homogeneous solution. Subsequently, 1 mmol $Co(NO_3)_2 \cdot 6H_2O$ and 2 mmol $Fe(NO_3)_3 \cdot 9H_2O$ were introduced into the above solution with rapid stirring for another 12 h. The resultant red-brown viscous liquid was loaded into a plastic syringe equipped with a 20-gauge needle that was electrically connected to a high voltage power supply. During the electrospinning process, the flow rate of solution was set at 1.0 mL h^{-1} controlled by a syringe pump. A high voltage of 18 KV was applied between the needle and the fiber collector, namely, aluminum foil. The distance between the needle tip and the aluminum foil was 18 cm. The as-spun fiber membrane was first stabilized in air at 250 °C for 3 h with the heating rate of 1 °C min^{-1}. Then the temperature was increased

to 600 °C with a heating rate of 5 °C min^{-1} and held for 3 h under N_2 atmosphere to obtain $CoFe_2O_4$@N-CNFs.

For comparison, pure $CoFe_2O_4$ and N-doped carbon nanofibers were also synthesized. For the synthesis of pure $CoFe_2O_4$, the as-obtained $CoFe_2O_4$@N-CNFs were calcinated at 600 °C in air for 3 h to completely remove the carbon. For the synthesis of N-CNFs, the synthetic protocol is similar to that for the synthesis of $CoFe_2O_4$@N-CNFs, without adding Co and Fe sources into the precursor.

Characterization: XRD measurements were performed on a Model D/max-rC X-ray diffractometer with Cu Kα radiation (λ = 1.5406 Å). TEM images and HRTEM images were acquired on a JEOL JEM-2100F transmission electron microscopy operated at an accelerating voltage of 200 kV. Energy dispersive spectrum (EDS), HAADF-STEM, and elemental mapping images were conducted on an FEI Tecnai G2 F20 microscope, which is built as an accessory on the JEOL JEM-2100F. Field-emission scanning electron microscopy images were taken on a JEOL JSM7500F. XPS measurements were conducted on a Thermo VG Scientific ESCALAB 250 spectrometer with an Al Kα radiator. TGA was carried out on a NetzschSTA449C thermal analyzer at a heating rate of 10 °C min^{-1} under air. The BET specific surface area was analyzed at 77 K by Micromeritics ASAP 2050 instrument.

Electrochemical Measurements: All electrochemical experiments were performed using a conventional three-electrode system on a CHI 660 electrochemical analyzer. In a three-electrode system, the catalyst-modified glassy carbon electrode (3 mm in diameter) was used as a working electrode, a Pt foil and a saturated calomel electrode served as the counter and reference electrode, respectively. The catalyst ink was prepared by ultrasonically dispersing the mixture of 4 mg of catalyst, 0.5 mL anhydrous ethanol, 1.5 mL distilled water, and 5 µL of 5 wt% Nafion solution. To immobilize the catalyst on the working electrode, 20 µL of the catalyst ink was dropped onto the glassy carbon electrode and dried under ambient condition. All electrochemical measurements were performed in N_2-saturated 0.1 M KOH solution, LSV tests were conducted at a sweep rate of 5 mV s^{-1} under 30 ± 1 °C.

Supporting Information

Supporting Information is available from the Wiley Online Library or from the author.

Acknowledgements

Conflict of Interest

The authors declare no conflict of interest.

Keywords

[1] H. Xu, J.-X. Feng, Y.-X. Tong, G.-R. Li, *ACS Catal.* **2017**, *7*, 986.
[2] M. Al-Mamun, Y. Wang, P. Liu, Y. L. Zhong, H. Yin, X. Su, H. Zhang, H. Yang, D. Wang, Z. Tang, H. Zhao, *J. Mater. Chem. A* **2016**, *4*, 18314.
[3] C.-Z. Yuan, Z.-T. Sun, Y.-F. Jiang, Z.-K. Yang, N. Jiang, Z.-W. Zhao, U. Y. Qazi, W.-H. Zhang, A.-W. Xu, *Small* **2017**, *13*, 1604161.
[4] X. Xiao, C.-T. He, S. Zhao, J. Li, W. Lin, Z. Yuan, Q. Zhang, S. Wang, L. Dai, D. Yu, *Energy Environ. Sci.* **2017**, *10*, 893.
[5] H. Chen, Y. Gao, L. Sun, *ChemSusChem* **2017**, *10*, 1475.
[6] J. Liang, Y.-Z. Wang, C.-C. Wang, S.-Y. Lu, *J. Mater. Chem. A* **2016**, *4*, 9797.
[7] R. Li, D. Zhou, J. Luo, W. Xu, J. Li, S. Li, P. Cheng, D. Yuan, *J. Power Sources* **2017**, *341*, 250.
[8] L. Xu, Qi. Jiang, Z. Xiao, X. Li, J. Huo, S. Wang, L. Dai, *Angew. Chem.* **2016**, *128*, 5363.
[9] J. Ping, Y. Wang, Q. Lu, B. Chen, J. Chen, Y. Huang, Q. Ma, C. Tan, J. Yang, X. Cao, Z. Wang, J. Wu, Y. Ying, H. Zhang, *Adv. Mater.* **2016**, *28*, 7640.
[10] Z. Xiao, Z. Huang, L. Xu, D. Yan, J. Huo, S. Wang, *Chem. Commun.* **2016**, *52*, 13008.
[11] H. Qian, J. Tang, Z. Wang, J. Kim, J. H. Kim, S. M. Alshehri, E. Yanmaz, X. Wang, Y. Yamauchi, *Chem. Eur. J.* **2016**, *22*, 1.
[12] X. Gao, H. Zhang, Q. Li, X. Yu, Z. Hong, X. Zhang, C. Liang, Z. Lin, *Angew. Chem., Int. Ed.* **2016**, *55*, 6290.
[13] C. Zhu, S. Fu, D. Du, Y. Lin, *Chem. Eur. J.* **2016**, *22*, 4000.
[14] J. Bao, X. Zhang, B. Fan, J. Zhang, M. Zhou, W. Yang, X. Hu, H. Wang, B. Pan, Y. Xie, *Angew. Chem., Int. Ed.* **2015**, *54*, 7399.
[15] M. Prabu, K. Ketpang, S. Shanmugam, *Nanoscale* **2014**, *6*, 3173.
[16] Z. Xu, S. C. Yan, Z. Shi, Y. F. Yao, P. Zhou, H. Y. Wang, Z. G. Zou, *ACS Appl. Mater. Interfaces* **2016**, *8*, 12887.
[17] C.-C. Lin, C. C. L. McCrory, *ACS Catal.* **2016**, *7*, 443.
[18] X.-F. Lu, L.-F. Gu, J.-W. Wang, J.-X. Wu, P.-Q. Liao, G.-R. Li, *Adv. Mater.* **2017**, *29*, 1604437.
[19] Y. Liu, J. Li, F. Li, W. Li, H. Yang, X. Zhang, Y. Liu, J. Ma, *J. Mater. Chem. A* **2016**, *4*, 4472.
[20] M. Al-Mamun, X. Su, H. Zhang, H. Yin, P. Liu, H. Yang, D. Wang, Z. Tang, Y. Wang, H. Zhao, *Small* **2016**, *12*, 2866.
[21] C. Sun, J. Yang, Zi. Dai, X. Wang, Y. Zhang, L. Li, P. Chen, W. Huang, X. Dong, *Nano Res.* **2016**, *9*, 1300.
[22] Z. Q. Liu, H. Cheng, N. Li, T. Y. Ma, Y. Z. Su, *Adv. Mater.* **2016**, *28*, 3777.
[23] X. Sun, X. Zhu, X. Yang, J. Sun, Y. Xia, D. Yang, *Green Energy Environ.* **2017**, *2*, 160.
[24] X. Yan, Y. Jia, J. Chen, Z. Zhu, X. Yao, *Adv. Mater.* **2016**, *28*, 8771.
[25] G. L. Tian, M. Q. Zhao, D. Yu, X. Y. Kong, J. Q. Huang, Q. Zhang, F. Wei, *Small* **2014**, *10*, 2251.
[26] Y. Zhao, R. Nakamura, K. Kamiya, S. Nakanishi, K. Hashimoto, *Nat. Commun.* **2013**, *4*, 2390.
[27] L. Li, S. Peng, Y. Cheah, P. Teh, J. Wang, G. Wee, Y. Ko, C. Wong, M. Srinivasan, *Chem. Eur. J.* **2013**, *19*, 5892.
[28] Y. J. Hong, J.-W. Yoon, J.-H. Lee, Y. C. Kang, *Chem. Eur. J.* **2015**, *21*, 371.
[29] H. Chen, G. Jiang, W. Yu, D. Liu, Y. Liu, L. Li, Q. Huang, Z. Tong, *J. Mater. Chem. A* **2016**, *4*, 5958.
[30] H.-F. Wang, C. Tang, X. Zhu, Q. Zhang, *J. Mater. Chem. A* **2016**, *4*, 3379.
[31] H. Zhu, D. Yu, S. Zhang, J. Chen, W. Wu, M. Wan, L. Wang, M. Zhang, M. Du, *Small* **2017**, *13*, 1700468.
[32] X. Wang, K. Cao, Y. Wang, L. Jiao, *Small* **2017**, *13*, 1700873.
[33] M. Prabu, K. Ketpang, S. Shanmugam, *Nanoscale* **2014**, *6*, 3173.
[34] S. Qiu, L. Xiao, M. L. Sushko, K. S. Han, Y. Shao, M. Yan, X. Liang, L. Mai, J. Feng, Y. Cao, X. Ai, H. Yang, J. Liu, *Adv. Energy Mater.* **2017**, *7*, 1700403.
[35] C. Li, Z. Y. Wu, H. W. Liang, J. F. Chen, S. H. Yu, *Small* **2017**, *13*, 1700453.

**ADVANCED
SCIENCE NEWS**

www.advancedsciencenews.com

**ADVANCED
SCIENCE**
Open Access

www.advancedscience.com

[36] X. Yan, K. Liu, T. Wang, Y. You, J. Liu, P. Wang, X. Pan, G. Wang, J. Luo, J. Zhu, *J. Mater. Chem. A* **2017**, *5*, 3336.

[37] D. Su, M. Cortie, G. Wang, *Adv. Energy Mater.* **2017**, *7*, 1602014.

[38] S. Gupta, S. Zhao, O. Ogoke, Y. Lin, H. Xu, G. Wu, *ChemSusChem* **2017**, *10*, 774.

[39] A. Al-Enizi, A. Elzatahry, A. Abdullah, A. Vinu, H. Iwai, S. Al-Deyab, *Appl. Surf. Sci.* **2017**, *401*, 306.

[40] X. Li, Y. Zhao, Y. Bai, X. Zhao, R. Wang, Y. Huang, Q. Liang, Z. Huang, *Electrochim. Acta* **2017**, *230*, 445.

[41] Y. Liu, N. Zhang, C. Yu, L. Jiao, J. Chen, *Nano Lett.* **2016**, *16*, 3321.

[42] T. Y. Ma, S. Dai, M. Jaroniec, S. Z. Qiao, *Angew. Chem., Int. Ed.* **2014**, *53*, 7281.

[43] J. Wang, F. Ciucci, *Small* **2017**, *13*, 1604103.

[44] S. Chen, J. Duan, M. Jaroniec, S. Z. Qiao, *Adv. Mater.* **2014**, *26*, 2925.

[45] P. Li, H. C. Zeng, *Adv. Funct. Mater.* **2017**, *27*, 1606325.

[46] C. C. L. McCrory, S. Jung, J. C. Peters, T. F. Jaramillo, *J. Am. Chem. Soc.* **2013**, *135*, 16977.

[47] N. Han, F. Zhao, Y. Li, *J. Mater. Chem. A* **2015**, *3*, 16348.

[48] J. Yang, G. Zhu, Y. Liu, J. Xia, Z. Ji, X. Shen, S. Wu, *Adv. Funct. Mater.* **2016**, *26*, 4712.

1700226 (9 of 9)